DOI: 10.1002/((please add manuscript number))
Article type: Communication

Solvent-Induced Self-Assembly Strategy to Synthesize Well-Defined Hierarchically Porous Polymers

Tu-Nan Gao, † *Tao Wang,* † *Wei Wu, Yali Liu, Qisheng Huo, Zhen-An Qiao* and Sheng Dai*

T.-N. Gao, Dr. T. Wang, W. Wu, Y. Liu, Prof. Q. S. Huo, Prof. Z.-A. Qiao
State Key Laboratory of Inorganic Synthesis and Preparative Chemistry, Jilin University
Changchun, Jilin 130012 (China)
E-mail: qiaozhenan@jlu.edu.cn

Prof. S. Dai
Chemical Sciences Division, Oak Ridge National Laboratory, Oak Ridge, Tennessee, 37831 (USA)
† These authors contributed equally to this work.
Keywords: mesoporous material, hypercrosslinked polymer, solvent-induced self-assembly, hierarchical porous polymer, solvent-free catalytic

Abstract: Porous polymers with well-orchestrated nanomorphologies are useful in many fields, but high surface area, hierarchical structure, and ordered pores are difficult to be satisfied in one polymer simultaneously. Herein, a solvent-induced self-assembly strategy to synthesize hierarchical porous polymers with tunable morphology, mesoporous structure, and microporous pore wall is reported. The poly(ethylene oxide)-*b*-polystyrene (PEO-*b*-PS) diblock copolymer micelles are crosslinked via Friedel-Crafts reaction, which is a new way to anchor micelles into porous polymers with well-defined structure. Varying the polarity of the solvent has a dramatic effect upon the hydrophilic/hydrophobic interaction, and the self-assembly structure of PEO-*b*-PS can be tailored from aggregated nanoparticles to hollow spheres even mesoporous bulk. A morphological phase diagram is accomplished to systematically evaluate the influence of the composition of PEO-*b*-PS and the mixed solvent component on the pore structure and morphology of products. The hypercrosslinked hollow polymer spheres provide a confined microenvironment for the in-situ reduction of K_2PdCl_4 to ultrasmall Pd nanoparticles which exhibits excellent catalytic performance in solvent-free catalytic oxidation of hydrocarbons and alcohols.

Porous organic polymers, with high porosity and various functional groups, are vibrant materials in biomedicine, catalysis, energy storage and membrane separation.[1] In the past decade, a series of porous polymers with different structures have been developed, such as covalent organic frameworks (COFs), porous aromatic frameworks (PAFs), polymers of intrinsic microporosity(PIM), conjugated microporous polymers (CMPs), and hypercrosslinked polymers (HCPs).[2] Despite the excellent physical and chemical properties of products, the synthetic routes of porous polymers generally require drastic synthetic conditions, such as noble metal catalysts for CMPs, inert atmosphere for PAFs, PIMs, and CMPs, complicated monomers for COFs, which significantly compromise their applications in scale-up and industrial implementation. HCPs, prepared by a succinct Friedel-Crafts reaction, stand out as a kind of practical porous polymer because of the robust and economic synthesis, high porosity and excellent thermal stability.[3] HCPs with hollow structure have been reported as excellent carriers for nanosize separation and active substance loading due to the integrate multiple-level porosity and high mass-transfer efficiency.[1d, 4] However, the general nature of C-C coupling process, linking the monomers with strong covalent bonds, generally leads to dense microporous frameworks, which makes it difficult to control mesopores and macropores incorporated in HCPs frameworks.[5] Up to now, few methods have been developed to synthesize HCPs with well-defined nanomorphology and hierarchical pores. Tan et al. have reported a fabrication of hollow microporous organic capsules by using SiO_2 spheres as a sacrificial agent.[5b] Wu et al. have proposed a stepwise crosslinking strategy, which used a two-step crosslinking to retain 3D assemblies of PS spheres.[5a] Those methods acquire hard templates such as silica or polystyrene spheres, which cause a poor efficiency and economy. Recently, our group reported a synthesis of HCPs membranes with hierarchical porosity by using an in situ crosslinking strategy, showing an excellent gas separation property. [6] The mesopores and macropores in HCPs membranes are not uniform or ordered, and the pore size cannot be controlled precisely.

Herein, we demonstrate a solvent-induced self-assembly method to synthesize hypercrosslinked hierarchical porous polymers with tunable mesoporous structure and microporous pore wall via a simple Friedel-Crafts reaction (**Scheme 1**). Formaldehyde dimethyl acetal (FDA)/1,2-dichloroethane (DCE) mixed solvents were used as the crosslinker and structure-directing solvent, and poly(ethylene oxide)-*b*-polystyrene (PEO-*b*-PS) was used as the template and reaction precursor. Varying the polarity of the reaction system, hydrophilic/ hydrophobic interaction can be controlled to adjust the self-assembly structure of PEO-*b*-PS from aggregated nanoparticles to hollow spheres then to mesoporous bulk. The mesoporous bulk HCPs exhibit well-defined mesoporous structure and high surface area. Moreover, uniform hollow sphere HCPs can be also generated with ultra-high surface area up to 1123 $m^2\ g^{-1}$. By changing the length of PEO segments, the pore size of these samples can be tuned from 6 nm to 12nm. Hypercrosslinked hollow polymer spheres provide a microenvironment to encapsulate and confine the ultrasmall Pd nanoparticles.[7] The Pd/hHCPs catalyst exhibits excellent catalysis activity in solvent-free aerobic oxidation of aromatic alcohols, aliphatic alcohols and aromatics hydrocarbons.

Four kinds of diblock copolymers PEO-*b*-PS with different block length (denote as PEO_{117}-*b*-PS_{395}, PEO_{117}-*b*-PS_{307}, PEO_{117}-*b*-PS_{190} and PEO_{45}-*b*-PS_{190}) were synthesized by atom transfer radical polymerization (ATRP),[8] using a PEO-Br initiator to initiate polymerization of styrene. The molecular weight and degree of polymerization were verified by ^{1}H nuclear magnetic resonance (NMR) and gel permeation chromatography (GPC). We take PEO_{117}-*b*-PS_{395} as the representative in the following discussion. The solution self-assembly of PEO-*b*-PS can be readily controlled by varying the nature of the solvent.[9] Optical photograph of PEO_{117}-*b*-PS_{395} in FDA reveals a colloid solution with Tyndall effect, and micelles of PEO_{117}-*b*-PS_{395} in FDA can be directly observed in TEM image (**Figure S1**). PEO_{117}-*b*-PS_{395} in DCE exhibits a clear solution (**Figure 1d**), indicating different self-assembly states in these two solvents. To shed light on the solvent-induced system, we designed a series of controlled experiments for PEO_{117}-*b*-PS_{395} by varying the volume ratio of FDA to DCE from 10:0 to 0:10. After hypercrosslinking, the obtained samples were donated as mHCPs-x (mesoporous bulk), hHCPs-x (hollow spheres), HCPs-x (aggregated nanoparticles), wherein x is FDA volume proportion. When FDA acted as the only solvent, the obtained mesoporous bulk HCPs (donated as mHCPs-1) exhibited a uniform mesoporous morphology (Figure 1a). The mesopores array into a nearly ordered structure with about 12 nm in diameter. Abundant of micropores can be observed on the pore wall from the high resolution TEM (Figure 1a inset). In a FDA:DCE = 9:1 solvent system, the obtained mHCPS-0.9 reveals an intermediate state, containing both mesoporous bulk and hollow spheres (Figure S1). From hHCPs-0.8 to hHCPs-0.2, all the mesoporous bulks disappeared, instead by pure hollow sphere phase. TEM image of hHCPs-0.2 (Figure 1b) reveals hollow spheres with a void space about 12 nm in diameter and a shell about 3-4 nm in thick. The micropores in shell can be observed in high resolution TEM (Figure 1b inset). SEM image of hHCPs-0.2 (**Figure S2**) shows a spherical morphology. The diameter of the hollow spheres was about 20 nm. When DCE was used as the only solvent and crosslinker, the obtained product (HCPs-0) exhibited some aggregated nanoparticles about 18 nm (Figure 1c).

Detailed information of pore structure was evaluated by nitrogen adsorption-desorption. Nitrogen adsorption-desorption isotherms of mHCPs and hHCPs are all type-IV curves based on the classification of the International Union of Pure and Applied Chemistry (IUPAC), suggesting the existence of mesopores (Figure 1e). For mHCPs, the adsorption isotherms show an apparent capillary condensation step at relative pressure of 0.45-0.8, which corresponds to the mesopores of 12 nm based on Barrett-Joyner-Halenda (BJH) model (Figure 1f). For hHCPs, the hysteresis loop at relative pressure from 0.45 to 0.8 is provided by the spherule-accumulating scaffolds (5 nm), and the other hysteresis loop at relative pressure from 0.8 to 1.0 is provided by the hollow sphere interiors (12 nm). These two samples exhibit an adsorption capacity at relative pressure before 0.05, indicating abundant micropores in the pore wall of mHCPs or shell of hHCPs, which was a desired advantage for nanoreactors. From mHCPs-1 to hHCPs-0.2, BET surface area of HCPs increased from 439 $cm^2 g^{-1}$ to 793 $cm^2 g^{-1}$, and micropore surface calculated by t-plot method increased from 125 $cm^2 g^{-1}$ to 227 $cm^2 g^{-1}$, because the increasing of DCE leads to a higher cross-linking degree and a significant increase in surface area.[10] Pore volume of hHCPs are larger than that of mHCPs due to the hollow interior (Figure 1g). The structure of HCPs-0 reveals aggregated nanoparticles, which lead to the smallest pore volume and surface area in this series of experiments. Thus, changing the composition of solvents can induce the self-assembly state of the PEO-*b*-PS, accordingly generate HCPs with different pore structure and morphology.

The crosslinking polymerization by the Friedel-Crafts reaction was confirmed by Fourier transform infrared (FT-IR) spectroscopy and ^{13}C nuclear magnetic resonance (NMR). The FT-IR spectra of uncrosslinked PEO-*b*-PS shows four peaks appearing at 1650-2000 cm^{-1}, assigned to monosubstituted benzene rings (**Figure S5**). After crosslinking, the four peaks between 1650-2000 cm^{-1} are replaced by one peak at 1675 cm^{-1}, which is attributed to tetrasubstituted benzene, indicating the successful crosslinking of PEO-*b*-PS. Peaks near 1500, 1580, 1600 and 1100 cm^{-1} are attributed to benzene rings from polystyrene and ether bonds from polyethylene oxide, which demonstrates the integrity of PEO-*b*-PS. ^{13}C NMR spectra of uncrosslinked PEO-*b*-PS was recorded with $CDCl_3$ as solvent (Figure 1h). The resonance peaks at 125 and 128 ppm represent the benzene rings on PS blocks, the resonance peak near 40 ppm could be attributed to the ethylene chain on PS, and the peak near 70ppm is originated from the oxethyl carbon on PEO. In the NMR of crosslinked PEO-*b*-PS, the peaks near 130 and 70 ppm have not changed, indicating the complete reservation of diblock copolymer. A new resonance peak at 55ppm is originated from the methoxy carbon on the benzene rings, which tallies with the Friedel-Crafts process. Compared with uncrosslinked PEO-*b*-PS, HCPs have a significant improvement on thermal stability due to the linking between benzene rings. Thermogravimetric analysis (TGA) suggests the weight loss of HCPs under nitrogen atmosphere at 800 °C is about 30%-70% (which is almost 100% in uncross-linked PEO-*b*-PS) varied from the different degrees of crosslinking, indicating the excellent thermal stability of HCPs (Figure S5). CHNSO element analyses of HCPs indicate a carbon element content of 80.3%, hydrogen element content of 6.6% and oxygen element content of 8.6% which is fitted with the elemental composition of PEO-*b*-PS (Table S1). Thus, the Friedel-Crafts reaction successfully happened and both PEO blocks and PS blocks were survived after the reaction.

Besides the solvents, the length of PS and PEO blocks also have an influence on the morphology and pore structure of HCPs. We synthesized diblock copolymer with shorter PEO blocks for more detailed information about the solvent-induced system. TEM images of mHCPs made by PEO_{45}-*b*-PS_{190} (**Figure 2a**) reveal an ordered mesoporous bulk structure with smaller pore size (6 nm) than that of mHCPs synthesized by PEO_{117}-*b*-PS_{395}. By increasing DCE, hollow sphere polymer was generated. Owing to the shorter PEO chains, hHCPs synthesized by PEO_{45}-*b*-PS_{190} (Figure 2b) exhibit a smaller hollow void space (6 nm) and diameter (12 nm) than hHCPs made by PEO_{117}-*b*-PS_{395}. This phenomenon suggests the longer PEO blocks lead to a larger pore size. We also reduced the length of PS chains for further investigation. When using FDA as the only solvent, PEO_{117}-*b*-PS_{307} exhibits unordered mesoporous bulk and hollow spheres after hypercrosslinking (Figure 2c), while hypercrosslinked PEO_{117}-*b*-PS_{190} exhibits a hollow sphere structure (**Figure S4**). With the FDA proportion decreased from 1 to 0.8, TEM images suggests both hypercrosslinked PEO_{117}-*b*-PS_{307} and PEO_{117}-*b*-PS_{190} assemble into hollow spheres (Figure S4). When the FDA proportion was 0, the hollow spheres totally disappeared, replaced by aggregated nanoparticles (Figure S4). The different self-assembly state indicates that PS block can influence the self-assembly structure, and copolymers with shorter PS blocks are easier to assemble into hollow sphere structure. We also designed a series of experiments to estimate the concentrations dependence of PS-*b*-PEO on morphologies of HCPs. However, the concentration of PS-*b*-PEO varying from 10 to 20 mg mL^{-1} has little influence on the products, and the morphologies of those HCPs are almost the same (Figure S7, Supporting Information).

We summarized a phase diagram based on a series of controlled experiments, and found that the chemical composition of diblock copolymers and solvent determine morphology of HCPs together (Figure 2e). The volume fraction of these four copolymers was calculated as PEO_{45}-*b*-PS_{190} (90.9%), PEO_{117}-*b*-PS_{395} (89.9%), PEO_{117}-*b*-PS_{307} (87.2%) and PEO_{117}-*b*-PS_{190} (81.1%) respectively. The volume fraction of PS block is similar in PEO_{45}-*b*-PS_{190} (90.9%) and PEO_{117}-*b*-PS_{395} (89.9%), and these two copolymers can assemble into an order mesoporous structure in FDA. Copolymers with lower PS volume fraction (PEO_{117}-*b*-PS_{307} and PEO_{117}-*b*-PS_{190}) tend to assemble into hollow spherical morphology instead of mesoporous structure. By changing the volume ratio of FDA:DCE, polarity of the solvent can be varied to effect the self-assembly state of hydrophobic segment and hydrophilic segment. PS segment and PEO segment aggregate into different morphologies in different solvent polarity to delimit the two interfaces for a thermodynamics and kinetics steady state. [9] The Lippert-Mataga polarity parameter (Δf) is introduced to measure the orientational polarization of mixed solvent (calculation equation was given in Supporting Information). Pure DCE owns the highest polarity (Δf=0.228) among these controlled experiments, in which PEO-*b*-PS forms a solid inner particle via hydrophilic/hydrophobic interaction. The polarity of solvent decreases with the addition of FDA. During the FDA content between 0.2~0.8, folded PEO segments become the inside wall, and swelled PS segments become the outside wall to stabilize PEO segments to achieve a hollow sphere morphology, because FDA is a good solvent for PS but a poor solvent for PEO (Figure 2d). In pure FDA (Δf=0. 0.088), the enhanced hydrophilic and hydrophobic interactions accumulate the hollow spheres to share the shell and arrange into an ordered mesoporous structure. Copolymers with longer PS segment have higher swelling degree, which provides more opportunity for the hollow spheres to contact with each other. During the process of Friedel-Crafts reaction, the hollow spheres are fused by the hyper-crosslinking among different spheres, leading to the formation of mesoporous bulk HCPs. We also summarized BET surface area of these samples (Table S2). For all kinds of crosslinked copolymers, BET surface area of these samples also reveals a relationship between the solvent constitution and crosslinking degree (Figure 2f). With the increase of DCE proportion, the products reveal a significant increase on surface area. For the experiments in pure DCE, surface area of these samples reduced significantly, because of the aggregated nanoparticle structure. It is worth noting that hHCPs synthesized by PEO_{117}-*b*-PS_{190} in FDA proportion of 0.2 exhibits a very high surface area up to 1123 $m^2\ g^{-1}$. Thus, we can draw a conclusion that reaction system can be controlled by two parameters: PS volume fraction of copolymer and the FDA proportion. Copolymers with high PS volume fraction can assemble into mesoporous structure in pure FDA solvent. Hollow sphere and aggregated nanoparticle morphologies can be obtained by adjust the solvent constitution, and pore size can also be tailored via changing PEO block.

The HCPs hollow spheres provide a unique microenvironment (a hydrophobic shell and hydrophilic inner) which is an ideal carrier for loading metal catalyst. [7,11] Owing to the hydrogen bonding interaction between PEO and palladium species, the hollow polymer spheres can prevent the aggregation of Pd nanoparticles, hHCPs-0.2 with 1 wt% Pd were synthesized by an impregnating K_2PdCl_4 into hHCPs-0.2 and using H_2 to reduce the precursor (detailed synthesis was given in supporting information). TEM image of Pd/hHCPs-0.2 reveals Pd nanoparticles with size around 2-5 nm stabilized by the hHCPs-0.2 (**Figure 3a**). The XRD pattern of Pd/hHCPs-0.2 shows a reflection peak at $2\theta = 39.3°$ (Figure 3b), which can be assigned to (111) crystal plane of cubic palladium lattice. Mean size of Pd nanoparticles was 3 nm calculated by the Scherrer equation. Pd/mHCPs-1 gives an uneven distribution of Pd particles, because of the smaller micropore surface area. The Pd 3d X-ray photoelectron spectroscopy (XPS) of Pd/hHCPs-0.2 exhibits two asymmetric peaks related to

Pd $3d_{5/2}$ and Pd $3d_{3/2}$ core levels (Figure 3c). Peaks near 342.0 eV and 337.3 eV correspond to Pd^{2+} species, and peaks around 341.6 eV and 335.7 eV are attributed to Pd^0. As a classical and common transformation, oxidation of hydrocarbon or alcohol plays an important role in organic synthesis and chemical industry.[11] Solvent-free oxidation of benzyl alcohol can be used as a typical model reaction to investigate the catalytic activity of Pd/hHCPs-0.2. Due to the high surface area, hierarchical pore structure and small sized Pd nanoparticles, Pd/hHCPs-0.2 nanocatalyst exhibits much higher activity for alcohol than Pd/mHCPs-1. Pd/hHCPs-0.2 exhibits a high turnover frequencies (TOF) of 7194 h^{-1} in solvent-free oxidation of benzene alcohol with a high conversion of benzene alcohol (63.4%) and a high selectivity (94%) to benzaldehyde. Moreover, the oxidation of cinnamyl alcohol, 3-octanol and 1-octanol are also suitable for Pd/hHCPs. The conversion of 3-octanol in 24h is 32%, which is very high compare to the reported excellent catalysts under similar conditions.[7, 11] The stability of Pd/hHCPs-0.2 were confirmed by a 10-times recycling test (Figure 3d). The Pd/hHCPs-0.2 maintain a high conversion and selectivity on oxidation of benzyl alcohol after 10 cycles. By loading Pd on hHCPs-0.2, we successfully synthesize a new heterogeneous catalyst with highly stability and activity.

In summary, we developed a solvent-induced strategy to synthesize hierarchical porous polymers with well-defined pore structure. By changing the composition of solvent, the morphology of porous polymer can be tuned from well-aligned mesoporous bulk to hollow spheres. Pore size can also be tailored via changing the length of PEO blocks. A morphological phase diagram was accomplished based on the composition of PEO-*b*-PS against the mixed solvents content. The obtained HCPs are excellent host materials for noble metal nanoparticles. Pd loaded hollow polymer spheres can be used as nanoreactors for hydrocarbon and alcohol oxidation reaction, and exhibit excellent catalysis activity and selectivity. This strategy shed light on the controlling of porous polymers with well-defined structures, which can be potentially used in many fields such as gas storage, catalysis, drug delivery, and chemical separation.

Supporting Information

Supporting Information is available from the Wiley Online Library or from the author.

Acknowledgements

This work was supported by the Young Thousand Talented Program and the National Natural Science Foundation of China (21671073, 21621001, and 21671074), the "111" Project of the Ministry of Education of China (B17020), and Program for JLU Science and Technology Innovative Research Team.

Received: ((will be filled in by the editorial staff))
Revised: ((will be filled in by the editorial staff))
Published online: ((will be filled in by the editorial staff))

References

[1] a) S. Das, P. Heasman, T. Ben, S. Qiu, *Chem Rev.* **2017**, *117*, 1515-1563; b) D. Wu, F. Xu, B. Sun, R. Fu, H. He, K. Matyjaszewski, *Chem Rev.* **2012**, *112*, 3959-4015; c) J. Wei, Z. Sun, W. Luo, Y. Li, A. A. Elzatahry, A. M. Al-Enizi, Y. Deng, D. Zhao, *J. Am. Chem. Soc.* **2017**, *139*, 1706-1713; d) L. Zhou, Z. Zhuang, H. Zhao, M. Lin, D. Zhao, L. Mai, *Adv Mater* **2017**, *29*; 1602914. e) D. Wu, F. Xu, B. Sun, R. Fu, H. He, K. Matyjaszewski, *Chem Rev.* **2012**, *112*, 3959-4015; f) N. Huebsch, D. J. Mooney, *Nature* **2009**, *462*, 426; g) H. B. Yao, H. Y. Fang, X. H. Wang, S. H. Yu, *Chem Soc Rev* **2011**, *40*, 3764-3785; h) Q. Sun, Z. Dai, X. Meng, F.-S. Xiao, *Chem Soc Rev* **2015**, *44*, 6018-6034.

[2] a) S. Liu, F. Wang, R. Dong, T. Zhang, J. Zhang, X. Zhuang, Y. Mai, X. Feng, *Adv Mater.* **2016**, *28*, 8365-8370; b) H. Furukawa, O. M. Yaghi, *J. Am. Chem. Soc.* **2009**, *131*, 8875-8883; c) L. Shaohua, Z. Jian, D. Renhao, G. Pavlo, Z. Tao, Z. Xiaodong, M. Yiyong, L. Feng, H. Andreas, F. Xinliang, *Angew. Chem. Int. Ed.* **2016**, *55*, 12516-12521; d) W. Mai, B.

Sun, L. Chen, F. Xu, H. Liu, Y. Liang, R. Fu, D. Wu, K. Matyjaszewski, *J. Am. Chem. Soc.* **2015**, *137*, 13256-13259; e) C. D. Wood, B. Tan, A. Trewin, H. Niu, D. Bradshaw, M. J. Rosseinsky, Y. Z. Khimyak, N. L. Campbell, R. Kirk, E. Stöckel, A. I. Cooper, *Chem. Mater.* **2007**, *19*, 2034-2048; f) A. P. Côté, A. I. Benin, N. W. Ockwig, M. O'Keeffe, A. J. Matzger, O. M. Yaghi, *Science* **2005**, *310*, 1166-1170; g) B. Li, Y. Zhang, R. Krishna, K. Yao, Y. Han, Z. Wu, D. Ma, Z. Shi, T. Pham, B. Space, J. Liu, P. K. Thallapally, J. Liu, M. Chrzanowski, S. Ma, *J. Am. Chem. Soc.* **2014**, *136*, 8654-8660; h) N. B. McKeown, P. M. Budd, *Chem Soc Rev* **2006**, *35*, 675-683; i) S. S.-Y. Chui, S. M.-F. Lo, J. P. H. Charmant, A. G. Orpen, I. D. Williams, *Science* **1999**, *283*, 1148-1150; j) J. Jia-Xing, S. Fabing, T. Abbie, W. C. D., C. N. L., N. Hongjun, D. Calum, G. A. Y., R. M. J., K. Y. Z., C. A. I., *Angew. Chem. Int. Ed.* **2007**, *46*, 8574-8578.

[3] a) H. Xu, J. Wu, B. Zheng, W. Mai, F. Xu, L. Chen, H. Liu, R. Fu, D. Wu, K. Matyjaszewski, *Chem Commun* **2017**, *53*, 5294-5297; b) L. Tan, B. Tan, *Chem Soc Rev* **2017**, *46*, 3322-3356; c) Z. Li, D. Wu, X. Huang, J. Ma, H. Liu, Y. Liang, R. Fu, K. Matyjaszewski, *Energy Environ. Sci.* **2014**, *7*, 3006; d) B. Li, R. Gong, W. Wang, X. Huang, W. Zhang, H. Li, C. Hu, B. Tan, *Macromolecules* **2011**, *44*, 2410-2414; e) A. H. Groschel, A. H. Muller, *Nanoscale* **2015**, *7*, 11841-11876; f) K. Wang, L. Huang, S. Razzaque, S. Jin, B. Tan, *Small* **2016**, *12*, 3134-3142; g) M. Seo, S. Kim, J. Oh, S.-J. Kim, M. A. Hillmyer, *J. Am. Chem. Soc.* **2015**, *137*, 600-603; h) Z. He, M. Zhou, T. Wang, Y. Xu, W. Yu, B. Shi, K. Huang, *ACS Appl. Mater. Interfaces* **2017**, *9*, 35209-35217.

[4] a) Z. Jia, K. Wang, B. Tan, Y. Gu, *ACS Catal.* **2017**, *7*, 3693-3702; b) X. Yang, K. Song, L. Tan, I. Hussain, T. Li, B. Tan, *Macromol. Chem. Phys.* **2014**, *215*, 1257-1263.

[5] a) H. Liu, S. Li, H. Yang, S. Liu, L. Chen, Z. Tang, R. Fu, D. Wu, *Adv Mater* **2017**, *29*; b) B. Li, X. Yang, L. Xia, M. I. Majeed, B. Tan, *Sci Rep* **2013**, *3*, 2128.

[6] Z. A. Qiao, S. H. Chai, K. Nelson, Z. Bi, J. Chen, S. M. Mahurin, X. Zhu, S. Dai, *Nat Commun* **2014**, *5*, 3705.

[7] Z. A. Qiao, P. Zhang, S. H. Chai, M. Chi, G. M. Veith, N. C. Gallego, M. Kidder, S. Dai, *J. Am. Chem. Soc.* **2014**, *136*, 11260-11263.

[8] a) Y. Deng, T. Yu, Y. Wan, Y. Shi, Y. Meng, D. Gu, L. Zhang, Y. Huang, C. Liu, X. Wu, D. Zhao, *J. Am. Chem. Soc.* **2007**, *129*, 1690-1697; b) A. H. Groschel, A. Walther, *Angew. Chem. Int. Ed.* **2017**, *56*, 10992-10994; c) H. Hu, M. Gopinadhan, C. O. Osuji, *Soft Matter* **2014**, *10*, 3867-3889; d) Y. Li, J. Wei, W. Luo, C. Wang, W. Li, S. Feng, Q. Yue, M. Wang, A. A. Elzatahry, Y. Deng, D. Zhao, *Chem. Mater.* **2014**, *26*, 2438-2444; e) W. Luo, T. Zhao, Y. Li, J. Wei, P. Xu, X. Li, Y. Wang, W. Zhang, A. A. Elzatahry, A. Alghamdi, Y. Deng, L. Wang, W. Jiang, Y. Liu, B. Kong, D. Zhao, *J. Am. Chem. Soc.* **2016**, *138*, 12586-12595.

[9] a) Y. Wang, J. He, C. Liu, W. H. Chong, H. Chen, *Angew. Chem. Int. Ed.* **2015**, *54*, 2022-2051; b) D. E. Discher, A. Eisenberg, *Science* **2002**, *297*, 967-973; c) Y. Mai, A. Eisenberg, *Chem Soc Rev* **2012**, *41*, 5969-5985; d) Z. Lin, S. Liu, W. Mao, H. Tian, N. Wang, N. Zhang, F. Tian, L. Han, X. Feng, Y. Mai, *Angew. Chem. Int. Ed.* **2017**, *56*, 7135-7140

[10] S. Wang, C. Zhang, Y. Shu, S. Jiang, Q. Xia, L. Chen, S. Jin, I. Hussain, A. I. Cooper, B. Tan, *Sci. Adv.* **2017**, *3*, 1602610.

[11] a) T. Wang, P. Zhang, Y. Sun, B. Liu, Y. Liu, Z.-A. Qiao, Q. Huo, S. Dai, *Chem. Mater.* **2017**, *29*, 4044-4051; b) C. Wang, L. Wang, J. Zhang, H. Wang, J. P. Lewis, F. S. Xiao, *J. Am. Chem. Soc.* **2016**, *138*, 7880-7883. (c) Enache D. I., Edwards J. K., Landon P., Solsona-Espriu B. Carley, A. F., Herzing A. A., Watanabe M., Kiely C. J., Knight D. W.,Hutchings G. J., Science 2006, 311, 362. (d) P. F Zhang., Y. T. Gong, H. R. Li, Z. R. Chen, Y. Wang, Nat. Commun. 2013, 4, 1593.

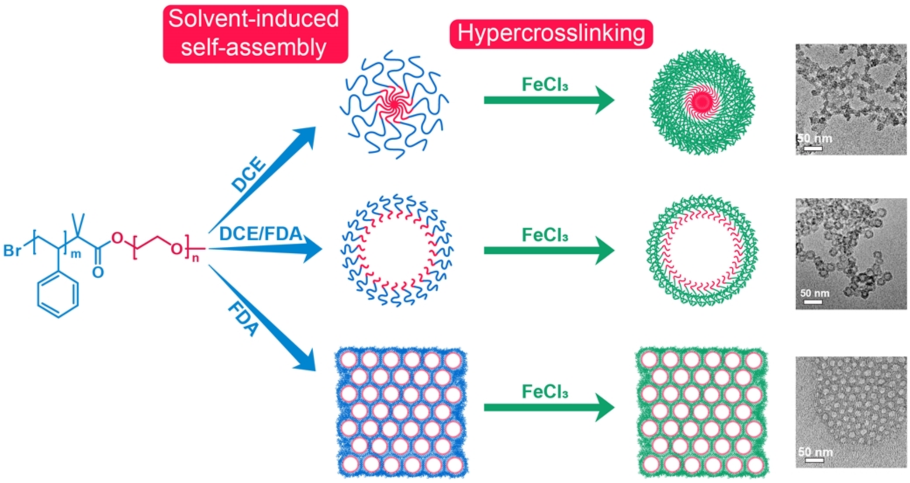

Scheme 1. Scheme illustration of controlled self-assembly and hyper-crosslinking of PS-*b*-PEO

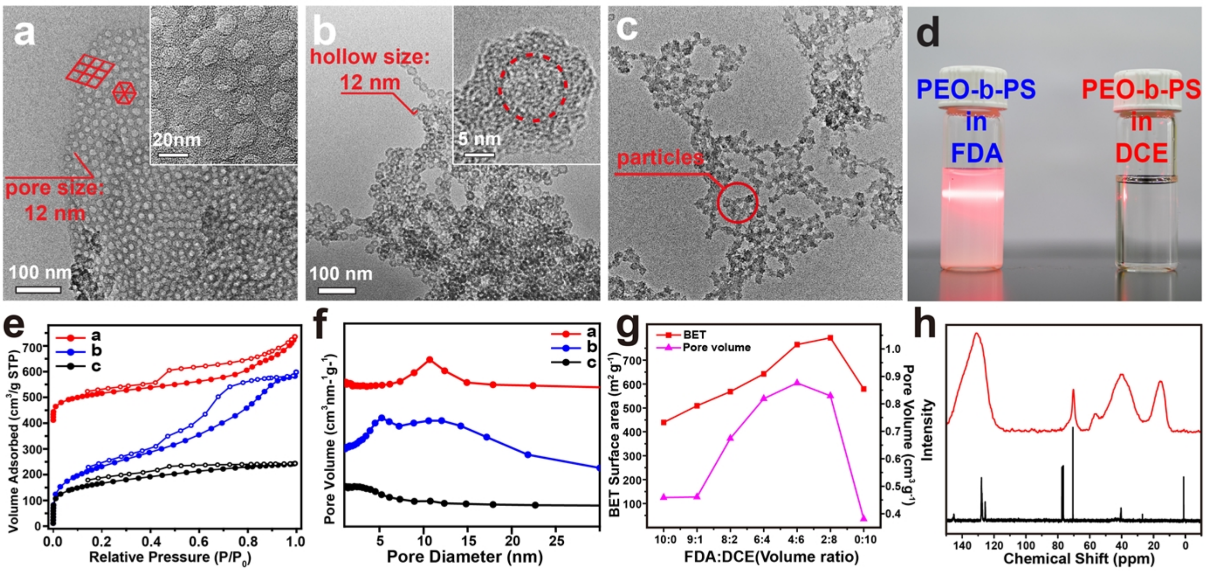

Figure 1. Structure control of the HCPs. TEM images of a) mHCPs-1, b) hHCPs-0.2, c) HCPs-0 , d) Optical photograph of PEO-*b*-PS in FDA and DCE respectively , d) mesoporous bulk HCPs synthesized with PEO_{45}-*b*-PS_{190}, e) Nitrogen adsorption-desorption isotherm of mesoporous bulk and hollow sphere, a was shifted to 400 $cm^2\ g^{-1}$, a-mHCPs-1, b-hHCPs-0.2, c-HCPs-0, f) Pore size distribution of HCPs, a-mHCPs-1, b-hHCPs-0.2, c-HCPs-0, g) Relationship between solvent ratio and pore volume of HCPs, Relationship between solvent content and BET surface area of HCPs, h) CP/MAS NMR spectrum of crosslinked and uncrosslinked PEO-*b*-PS

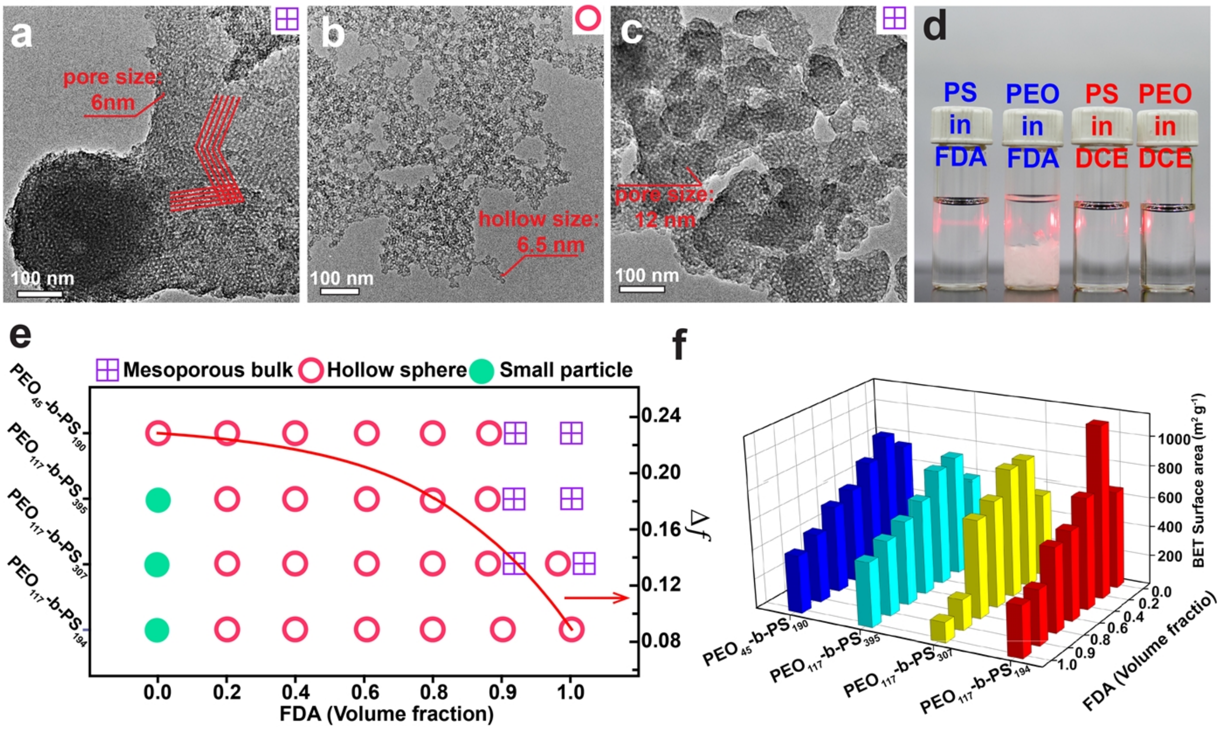

Figure 2. a) TEM image of mesoporous bulk HCPs synthesized with PEO_{45}-*b*-PS_{190}, b) hollow sphere HCPs synthesized with PEO_{45}-*b*-PS_{190}. c) mesoporous bulk HCPs synthesized with PEO_{117}-*b*-PS_{307} d) Optical photograph of PS and PEO in different solvents, e) Morphological phase diagram based on the composition of PS-*b*-PEO against the mixed solvents content and Lippert-Mataga polarity parameter against the mixed solvents content, f) Summary of BET surface area of all the simples

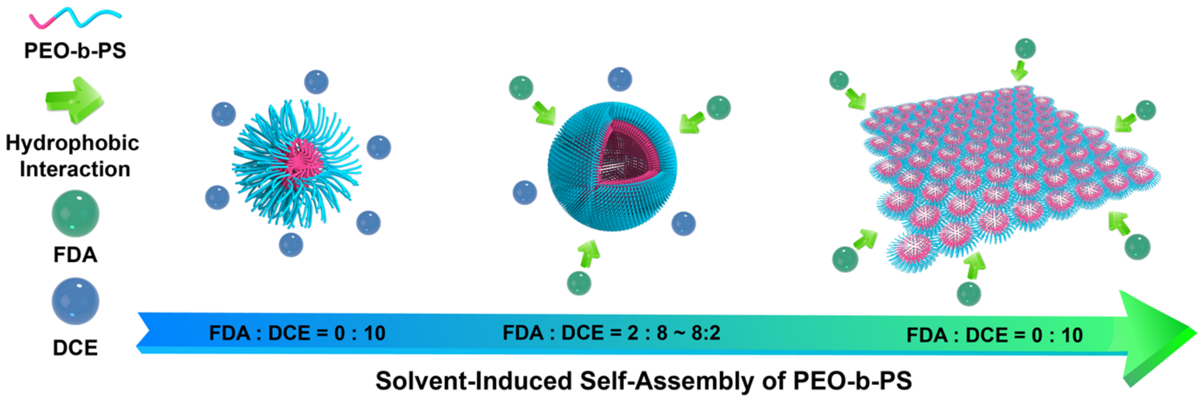

Scheme 2. Scheme illustration of proposed formation mechanism for the solvent-induced system

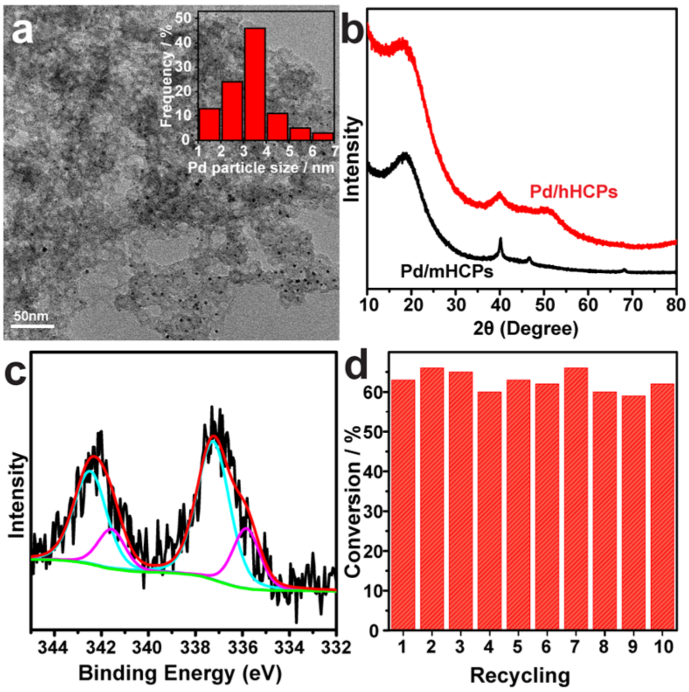

Figure 3. a) TEM image of Pd/hHCPs. b) XRD pattern of Pd/hHCPs and Pd/mHCPs, c) XPS spectra of Pd/hHCPs-0.2, d) recycling test of Pd/hHCPs-0.2 in the benzyl alcohol oxidation.

Table 1. Oxidation of alcohol and hydrocarbon catalyzed by Pd/hHCPs with O_2.[a]

Entry	Subtrate	Temp. (℃)	Product		TOF[b]	Conv. (%)
1	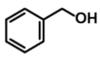	120	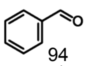 94	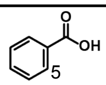 5	7194	63.4
2[c]	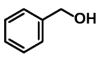	120	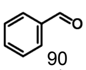 90	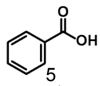 5	2883	41
3	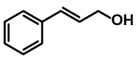	120	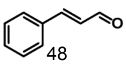 48	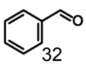 32	4129	42.1
4	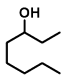	140	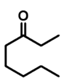	99	4010	32
5	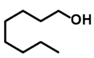	140	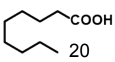 20	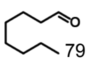 79	534	4.2
6	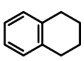	100	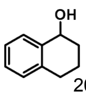 20	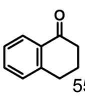 55	790	45.2
7	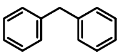	120	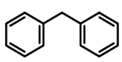 99		2026	19.1

[a] Reaction conditions : 10 mg of substrate, 10 mg of Pd/hHCPs, O_2 1 atm.
[b] TOF = [reacted mol substrate]/[(total mol metal)×(reaction time)]. The TOFs were measured after first 0.5 h of reaction.
[c] The oxidation was performed with Pd/mHCPs as catalyst.

Solvent- induced strategy to synthesize hierarchical porous polymer, by varying polarity of the solvents,the self-assembly structure of PEO-*b*-PS can be tailored from aggregated nanoparticles to hollow spheres even mesoporous bulk.

Keyword mesoporous material, hypercrosslinked polymer, solvent-induced self-assembly, hierarchical porous polymer, solvent-free catalytic

T. N. Gao, T. Wang, W. Wu, Y. Liu, Z. A. Qiao* and S. Dai

Solvent-Induced Self-Assembly Strategy to Synthesize Well-Defined Hierarchical Porous Polymer